Contents

Van der Waals-like transition in fluidized granular matter

Rodrigo Soto, Médéric Argentina, and Marcel G. Clerc

Departamento de Física, Facultad de Ciencias Físicas y Matemáticas, Universidad de Chile, Casilla 487-3, Santiago, Chile.

Summary. A phase separation of fluidized granular matter is presented. Molecular dynamics simulations of a granular system, in two spatial dimensions, with a vibrating wall and without gravity exhibit appearance, coagulation, and evaporation of bubbles. The instability is produced by the existence of a negative compressibility region, that is caused by the energy dissipation at collisions. The phenomenon is analogous to the spinodal decomposition of the gas-liquid transition of the van der Waals model. A hydrodynamic model gives account for the negative compressibility and predicts a critical point that is in qualitative agreement with the results of the simulations. In the onset of phase separation, we have deduced a macroscopic model that agrees quite well with molecular dynamics simulations.

Granular matter, when fluidized by continuous energy injection exhibits a variety of phenomena that resembles those of molecular fluids: patterns and instabilities appear, Rayleigh-Benard like convection is developed, etc [1–3]. The main difference with molecular fluids is that, at collisions, grains dissipate kinetic energy into the internal degrees of freedom of the grains. Hence energy must be supplied continuously to sustain a fluidized regime. Experimentally, energy is usually injected through vibrating walls or by the gravitational field.

Fluidized granular systems have the tendency to create large gradients in the hydrodynamic fields, and microscopic and macroscopic time and length scales are not enough separated as in elastic fluids [4]. However, when dissipation is not too large, fluidized regimes of granular matter are described successfully using hydrodynamic models. These models are similar to the Navier-Stokes equations for elastic fluids, with the addition of an energy dissipation term.

Here, we describe a new type of instability observed in fluidized granular matter, analogous to the spinodal decomposition of the gas-liquid transition in the van der Waals model [5]. The instability was first predicted using a linear stability analysis of the hydrodynamic equations [6] and later in Ref. [7]. An nonlinear analysis, as well as the time evolution of the instability was performed by the authors in Ref. [8].

The origin of the instability relies on the fact that for granular media the average granular temperature is a decreasing function of the density for fixed boundary conditions (see later for a detailed explanation). This results in negative compressibility for dissipations larger than a critical value giving rise to a spatial instability. We also show that the instability can be understood using a simple hydrodynamic model.

We consider a two-dimensional system of grains on an horizontal surface, with friction ignored, placed in a box with large aspect ratio (see Fig. 1). Henceforth, we will refer to horizontal and vertical directions as the long and short directions, respectively; the system is periodic in the horizontal direction. The top wall reflects grains elastically while the bottom one injects energy into the system by means of a vibrating wall at high frequency ω and small amplitude A. The collisions with the wall are elastic with no friction, thus conserving horizontal momentum. Due to the high frequency, the collisions with the wall are uncorrelated, being modeled in a stochastic way. For simplicity, the vibrating wall is well modeled by a stochastic wall: each time a grain collides with the wall, it is reflected conserving the tangential component of the velocity, but the normal component is sorted from a Maxwellian distribution at a certain temperature, that scales as $T \sim m(A\omega)^2$, m being the mass of the gains [9]. We define the granular temperature (the *temperature* from now on), like in molecular fluids, to be proportional to the kinetic energy per particle in the reference frame of the fluid. We emphasize that both collisions with the walls and between the grains conserve horizontal momentum.

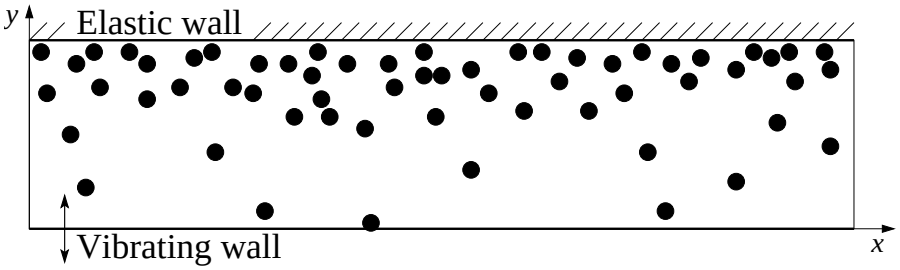

Fig. 1. Schematic representation of the studied system. Grains are placed in an horizontal box. The bottom wall is vibrating while the top one reflects grains elastically. The system is periodic in the x direction.

The system is studied using molecular dynamics simulations of the Inelastic Hard Sphere model (IHS) [10–12]. Grains are modeled as smooth rigid disks and the collisions are characterized by a constant normal restitution coefficient α. Grains only have translational degrees of freedom and there is no tangential friction between grains at collisions. The IHS has been widely studied and reproduces well many of the observed phenomena in granular fluids at moderate densities, where rotation is not fundamental (see, for ex-

ample, [10–12]). Units are chosen such that the diameter σ and mass m of each disk is one. Also, taking the wall temperature as one, energy units are fixed. Under these conditions, the system is completely defined by the total number of grains N, the aspect ratio $\lambda = L_x/L_y \gg 1$, the global number density $n_0 = N/(L_x L_y)$, and the restitution coefficient of the grains $\alpha = (1-2q)$; the elastic limit corresponds to $q = 0$.

At low dissipation, the granular media develops vertical density and temperature profiles induced by the dissipation at collisions and the energy injection mechanism, but both fields are homogeneous in the horizontal direction. The system is hotter and less dense near the injecting wall, and colder and denser by the opposite wall (see Fig. 1). For a detailed study of this state see Ref. [13].

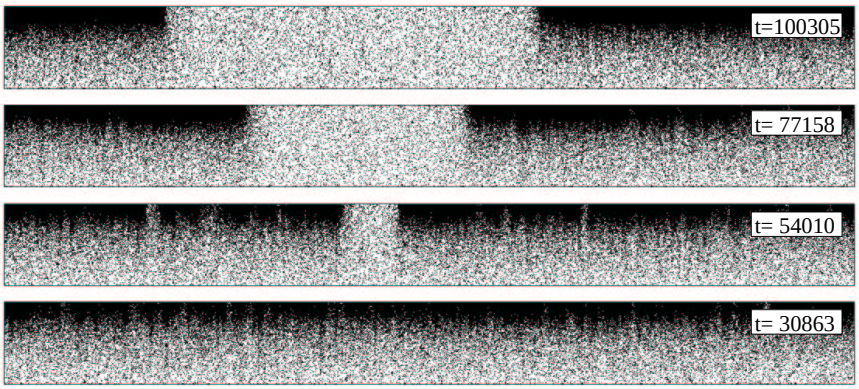

Fig. 2. Snapshots of a system with $N = 153600$, $\lambda = 102.4$, $n_0 = 0.15$, $L_x = 10240$, and $q = 0.02$. The configurations correspond to different simulation times. Each black dot represents a simulated grain and the aspect ratio has been distorted to make the system visible. The bubble appears at $t \approx 40000$.

For a larger dissipation ($N = 153600$, $\lambda = 102.4$, $n_0 = 0.15$, $L_x = 10240$, and $q = 0.02$) an spatial instability is observed: the system exhibits the coexistence of two fluid phases, characterized by different densities (see Fig. 2). Initially the fluid remains horizontally homogeneous and suddenly a bubble (low density region) appears and grows until it achieves its final size. After that, the system remains stationary with the two phases coexisting.

To characterize in more detail this instability, we analyze the temporal evolution of the vertically averaged density (*coarse grained density*) $\rho(x,t) = L_y^{-1} \int_0^{L_y} n(x,y,t)dy$, where $n(x,y,t)$ is the density field. In Fig. 3 the spatio-temporal evolution of $\rho(x,t)$ is presented. It is clearly seen that the system remains in a homogeneous state for a finite large time until the bubble is nucleated due to density fluctuations. Therefore, this homogeneous state is a

metastable one. Afterward, the bubble grows with a nearly constant velocity while two densification fronts propagate away from the bubble at a larger, but also constant, velocity (illustrated in Fig. 3). When the fronts reach the growing bubble —through the periodic boundary conditions— it is pushed inward, leading to damped oscillations in its size. Finally, the system achieves a stationary state with the bubble.

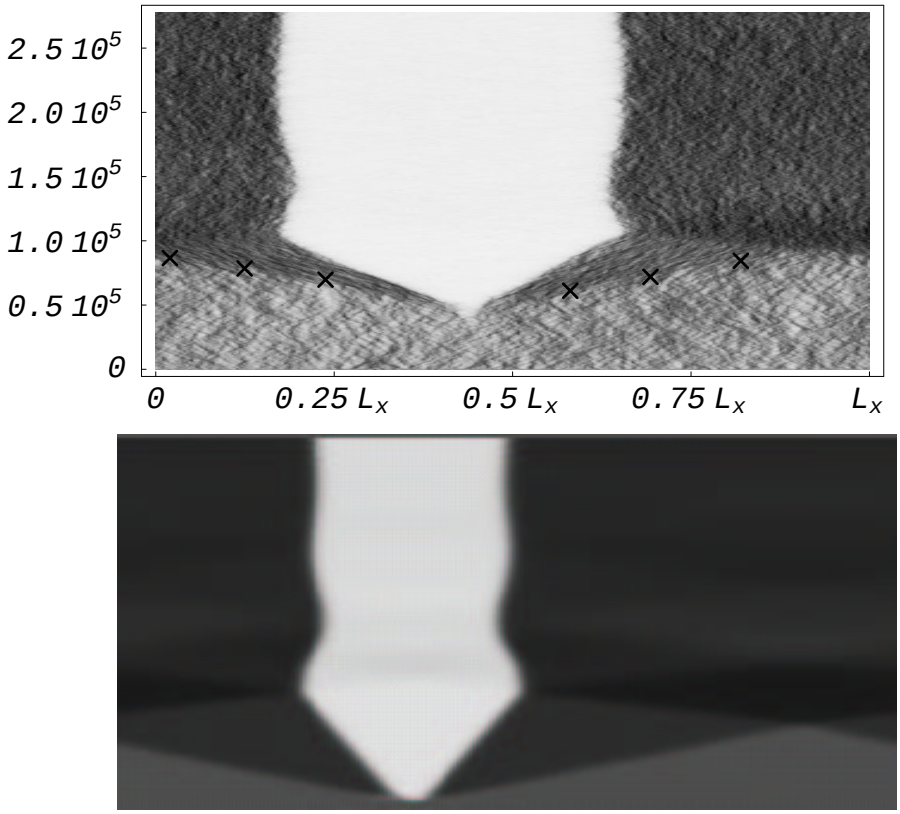

Fig. 3. Spatiotemporal evolution of the coarse grained density $\rho(x,t)$, with time on the vertical axis and increasing upward. The gray scale is proportional to density, with darker regions representing denser regions in the system. The top graph corresponds to the molecular dynamics simulation with the same parameters as in Fig. 2, where the bubble nucleation is triggered by internal noise. In the final state, the vertically averaged density of the bubble is $\rho = 0.025$, while in the dense region $\rho = 0.257$. The densification fronts are marked with lines of crosses. The bottom graph is obtained by the simulation of the model defined by Eq. (11) with $\varepsilon = -6.6 \times 10^{-4}$ and $\nu = 2$. The system size is 5400 and the total simulation is time $T = 3.5 \times 10^5$. An initial condition (with $u = 1.4 \times 10^{-2}$) that overcomes the nucleation barrier is imposed. The minimum (light gray) and maximum (dark gray) densities are $u = -2.6 \times 10^{-2}$ and $u = 2.9 \times 10^{-2}$, respectively.

The system shows a different behavior, according to the value of the dissipation parameter q. In Fig. 4 the spatiotemporal evolution of a system with a smaller dissipation is shown ($q = 0.01$). In this case four bubbles are created in the fluid with no apparent metastable time. Two of them merge into a single one, and later on, the smallest one disappears or evaporates. Later on the two remaining bubbles evolve slowly, one of them growing while the other one decreases. Densification fronts, created with the bubbles, are also seen.

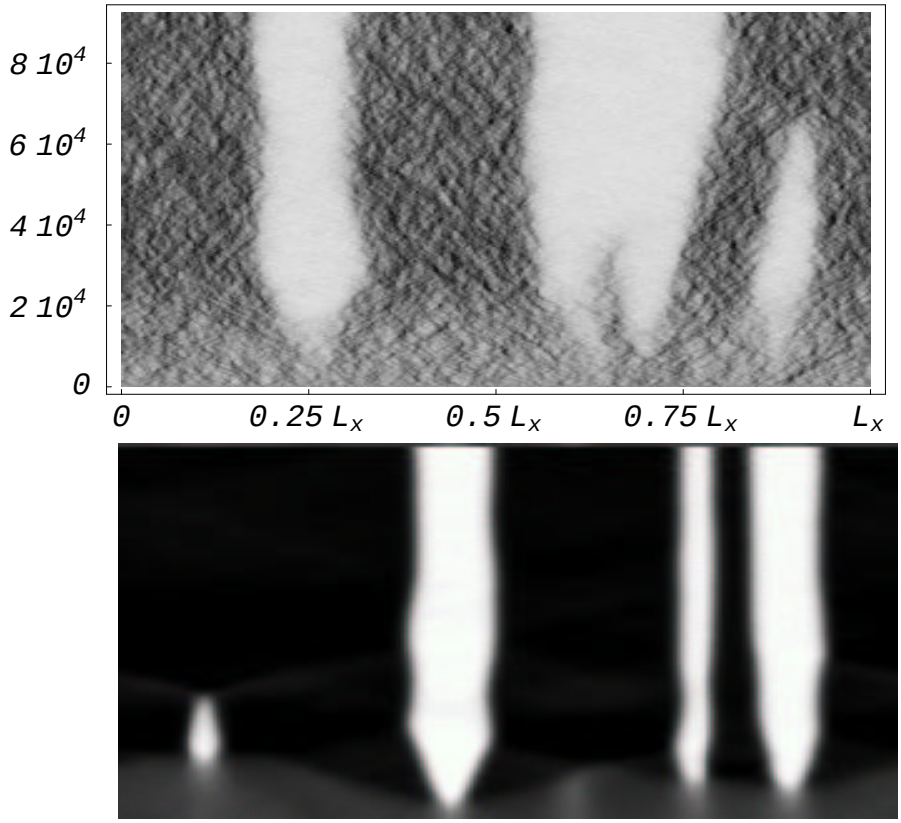

Fig. 4. The same representation as in Fig. 3, but changing the dissipation parameter to $q = 0.01$. In the final simulated state, the vertically averaged density of the bubbles is $\rho = 0.046$, while in the dense regions $\rho = 0.216$. In the bottom graph, we use the same parameters and gray scale as in Fig. 3 and the initial condition is $u = 7.4 \times 10^{-3}$. In this case there is no nucleation barrier and the initial condition used in the solution of the model is homogeneous with small fluctuations that are amplified by the instability.

We have also made a series of simulations keeping constant the value of q and changing the value of the global density n_0. All the simulations were

done with the following parameters $N = 153600$, $q = 0.02$, and $L_y = 100$. The spatio-temporal evolution of the coarse grained density $\rho(x,t)$ is represented in Fig. 5 for different values of n_0. For global densities smaller that $n_0 = 0.03$ the system remains stable; for densities between $n_0 = 0.033$ and $n_0 = 0.15$ the system is unstable or metastable and depending on the case low density regions (bubbles) or large density ones (droplets) are created; finally for densities larger than $n_0 = 0.25$ no instabilities were observed. Note that in all cases (specially visible for $n_0 = 0.03$) density waves created by density fluctuations are observed in the background regions. These waves propagate with well defined velocities.

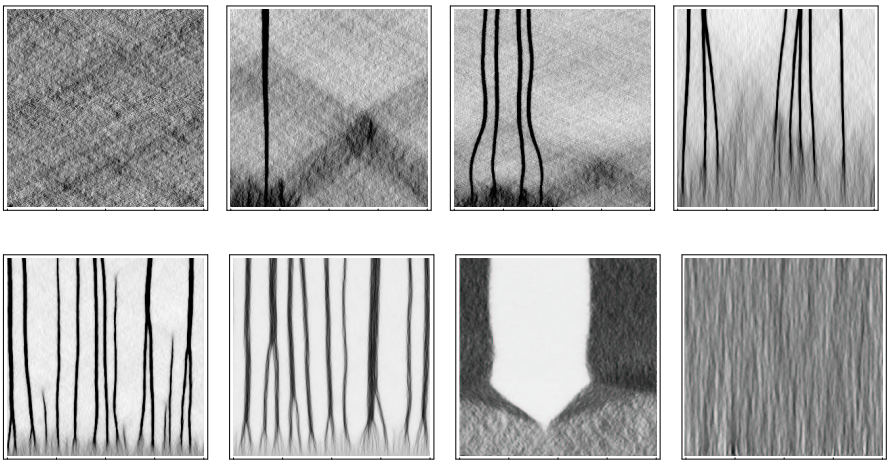

Fig. 5. Spatiotemporal evolution of the coarse grained density $\rho(x,t)$. All the simulations are done with $N = 153600$, $q = 0.02$, and $L_y = 100$. The simulations differ in the global density; from left to right and top to bottom the densities are $n_0 = 0.03, 0.033, 0.035, 0.04, 0.05, 0.08, 0.15$, and 0.30.

The observed behavior is similar to the van der Waals gas liquid transition, where for temperatures lower that the critical one, there is a density range for which the homogeneous state is unstable. Here, in the granular fluid, the control parameter is the dissipation coefficient q instead of the thermodynamic temperature.

The origin of the instability can be understood as follows. In thermodynamic equilibrium, the pressure is a monotonous increasing function of the density and the temperature [14]. But, in this system, the granular temperature adjusts itself to a stationary profile given by the energy balance between dissipation at collisions and injection at the vibrating wall. As the dissipation rate is proportional to density, the stationary temperature is a decreasing function of ρ. As an outcome, the effective pressure (that is independent of y due to the absence of gravity) can present a region where it decreases with

an increasing density. That is, the temperature drop produced by collisions can be large enough to give rise to a decrease in pressure when increasing the global density [15]. Then, there can be a region of negative compressibility ($\partial p_{xx}/\partial n_0 < 0$) in the same sense as the van der Waals loop in classical fluids, that triggers the instability.

The existence of the negative compressibility region can be verified numerically as follows. We have performed molecular dynamics simulations of the IHS system in tall boxes ($L_x \ll L_y$) to prevent the spatial instability to develop; when the horizontal system size is small, there is a large surface energy cost in creating a bubble, and the system remains stable. We compute the horizontal momentum flux ($x-x$ component of the pressure tensor, p_{xx}), averaged over the vertical direction for different values of the global density n_0 and the dissipation coefficient q. For constant q, the pressure p_{xx} exhibits the appearance of van der Waals loops, with a critical point located at $q \approx 0.0047$ and $n_0 \approx 0.15$ (see Fig. 6). For larger values of q there is a region with negative compressibility that is bounded by the spinodal curve. Also, we can compute the coexistence curve using Maxwell's construction. The region between the coexistence and spinodal curves define the metastability region, where bubbles or droplets can nucleate thanks to density fluctuations. Inside the spinodal curve, the system is mechanically unstable.

In the previous paragraph, we used concepts of equilibrium thermodynamics like surface energy and Maxwell's construction. Below we show that the system dynamics is described by a free energy (Landau type) allowing the use of this concepts.

The existence of the negative compressibility region can be studied theoretically using a hydrodynamic description of granular fluids [16]. In Ref. [17] the negative compressibility region was also observed, but due to the use of constitutive relations of dilute granular gases does there was no saturation.

Here we investigate the presence of the negative compressibility region with a different perspective. As in Ref. [16] we consider simple hydrodynamic equations that mimic the Navier-Stokes ones with a dissipation term in the energy equation, modeling the energy dissipation at collisions. For sufficiently small dissipation ($q \ll 1$), one has [18–21]

$$\begin{aligned}
&\frac{\partial n}{\partial t} + \nabla \cdot (n\vec{v}) = 0,\\
&n\left(\frac{\partial \vec{v}}{\partial t} + (\vec{v}\cdot\nabla)\vec{v}\right) = -\nabla\cdot \mathbb{P},\\
&n\left(\frac{\partial T}{\partial t} + (\vec{v}\cdot\nabla)T\right) = -\nabla\cdot\vec{J} - \mathbb{P} : \nabla\vec{v} - \omega,
\end{aligned} \tag{1}$$

with the usual constitutive equations for the pressure tensor (hydrostatic pressure and Newton's law) and the Fourier's law for the heat, and the new constitutive equation for the energy dissipation rate flux,

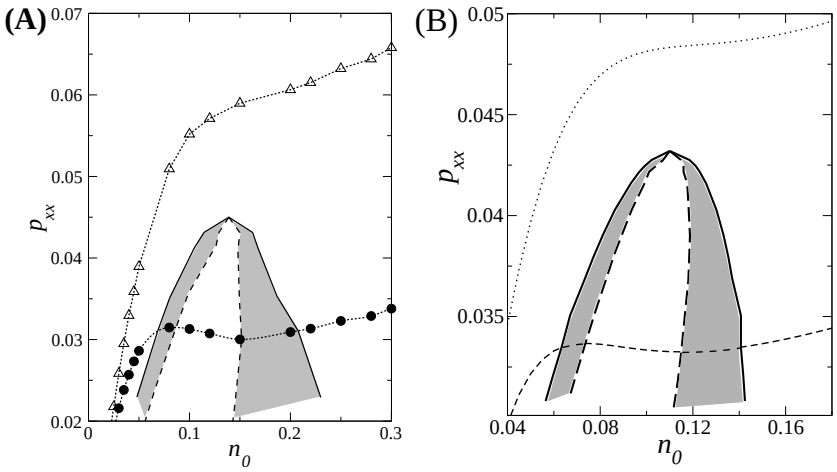

Fig. 6. (A) Phase diagram obtained from molecular dynamics simulations in tall, narrow boxes. The dotted curves correspond to the horizontal component of the pressure tensor p_{xx} for the dissipations $q = 0.0032$ (open triangles) and $q = 0.0070$ (filled circles), smaller and larger than the critical one, respectively. The second case presents a van der Waals loop. The coexistence curve (solid line) and spinodal curve (dashed line) are plotted. **(B)** Phase diagram obtained from the hydrodynamic model. The solid line (long-dashed) curve is the coexistence (spinodal) curve. The gray region is the metastability region. The dotted (short-dashed) curve correspond to the hydrodynamic pressure for the dissipation $q = 0.007$ ($q = 0.0130$).

$$\begin{aligned} I\!P_{i,j} =& p(n,T)\delta_{i,j} - \eta(n,T)\left(\frac{\partial v_i}{\partial x_j} + \frac{\partial v_j}{\partial x_i}\right) - (\xi(n,T) - \eta(n,T))\nabla\cdot\vec{v}\delta_{i,j} \\ \vec{J} =& -k(n,T)\nabla T \\ \omega =& \omega_0(n,T)n^2T^{3/2}. \end{aligned} \tag{2}$$

where p is the hydrostatic pressure, η is the shear viscosity, ξ is the bulk viscosity, k is the thermal conductivity, and ω_0 is a factor that accounts for the energy dissipation at collisions.

The transport coefficients in the limit of small dissipation are the same as for elastic spheres in 2D [22], except for the one associated to the energy dissipation, that is calculated directly using the Enskog theory [23]. All the transport coefficients are expressed in terms of the pair correlation function of elastic disks at contact, χ [23].

$$\chi(n) = \frac{1 - 7\pi n/64}{(1 - \pi n/4)^2} \tag{3}$$

$$p(n,T) = nT\frac{\left(1 + \pi^2 n^2/128\right)}{(1 - \pi n/4)^2} \tag{4}$$

$$\eta(n,T) = \frac{1}{2\chi}\left(1 + \pi n\chi/2 + 0.87(\pi n\chi/2)^2\right)\sqrt{\frac{T}{\pi}} \tag{5}$$

$$\xi(n,T) = \frac{1.246}{2\chi}(\pi n\chi/2)^2\sqrt{\frac{T}{\pi}} \tag{6}$$

$$k(n,T) = \frac{2}{\chi}\left(1 + 3\pi n\chi/4 + 0.87(\pi n\chi/2)^2\right)\sqrt{\frac{T}{\pi}} \tag{7}$$

$$\omega_0 = 4\sqrt{\pi}q\chi(n) \tag{8}$$

The use of hydrodynamic equations for describing granular fluids is controversial because hydrodynamic theory is based on the local tendency of fluids toward equilibrium, condition that is not necessarily satisfied in granular fluids. However, the use of kinetic theory give a support for this kind of description at least in the dilute and quasielastic case (see for example Refs. [18, 24]) . In this article we will not put into question the validity of the hydrodynamic model, and we will use it to obtain qualitative and quantitative predictions.

In the model (1), density and horizontal momentum satisfy conservation equations. We consider that the the velocity field is small enough to neglect nonlinear terms in $\vec{v}$. Density and horizontal momentum can be vertically averaged giving $\rho(x,t)$ and $j(x,t)$, that obey the equations

$$\partial_t \rho\,(x,t) = -\partial_x j\,(x,t)\,, \tag{9a}$$

$$\partial_t j\,(x,t) = -\partial_x \Phi, \tag{9b}$$

where Φ is the vertical average of the $x-x$ component of the pressure tensor.

Eqs. (9) show that the conserved fields ρ and j have an evolution given by a time scale proportional to the value of the horizontal gradients. When the horizontal gradients are much smaller than the vertical ones, ρ and j behave as the only slow variables and govern the system dynamics. The other fields (vertical momentum, temperature, and Φ) have fast dynamics and behave as slave variables of ρ and j, that is their values follow the evolution of the slow fields.

The value of Φ can be computed using the equations for the temperature and vertical momentum. The vertical momentum relaxes fast to its equilibrium value, zero, due to the boundary conditions. Then, the pressure is independent of y ($\Phi = p$). Energy is not conserved implying that temperature is also a fast variable and satisfies the equation $\nabla \cdot \vec{J} + \omega = 0$. The equations of T and Φ can be solved numerically with the boundary condi-

tions $T = 1$ at the bottom and $\vec{J} = 0$ at the top, and the integral condition $\int_0^{L_y} n(x, y, t)dy = L_y\, \rho(x, t)$.

For fixed q, the pressure exhibits, as proposed before, van der Waals loops as a function of $n_0 = \rho(x, t)$ (see Fig. 6). The negative compressibility region has a critical point at $q \approx 0.0086$ and $n_0 \approx 0.11$.

The results on the hydrodynamic model are in qualitative agreement with the molecular dynamics simulations in tall boxes. The difference is originated mainly in the boundary condition for T. Indeed, even though particles are forced to come out of the bottom wall with velocities characteristic of a temperature equal to 1, the granular temperature at the boundary is less than one because, due to dissipation, the particles that arrive at the wall come with a smaller kinetic energy. This is a well known effect in dilute gases (Knudsen layer effects [25]), that become also important in granular fluids.

Having verified that the mechanism that originates the instability is a negative compressibility in the effective pressure, we can describe the dynamics of the dominant mode near the bifurcation point (critical point in the van der Waals language). The critical point is defined by the condition that both $\partial\Phi/\partial\rho$ and $\partial^2\Phi/\partial\rho^2$ vanish. Using symmetry and scaling arguments it can be argued that the averaged pressure Φ close to the critical point can be written as (see Ref. [8])

$$\begin{aligned}\Phi \approx \Phi_o + \frac{\partial\Phi}{\partial\rho}\bar{\rho} + \frac{\partial^2\Phi}{\partial^2\rho}\frac{\bar{\rho}^2}{2} + \frac{\partial^3\Phi}{\partial^3\rho}\frac{\bar{\rho}^3}{6} + \frac{\partial\Phi}{\partial j^2}j^2 \\ + \frac{\partial\Phi}{\partial\rho_{xx}}\bar{\rho}_{xx} + \frac{\partial\Phi}{\partial j_x}j_x,\end{aligned} \tag{10}$$

where $\bar{\rho} = \rho - n_0$.

For sake of simplicity, we define now $u = \rho - \rho_M$, where ρ_M is the density at the Maxwell point (i.e. where $\partial^2\Phi/\partial^2\rho\big|_{\rho_M} = 0$). Scaling u and x, Eqs. (9) are approximated at the dominant order by the *Van der Waals normal form*

$$\begin{aligned}\partial_{tt}u &= \partial_{xx}\left(\varepsilon u + u^3 - \partial_{xx}u + \nu\partial_t u\right), \\ &= \partial_{xx}\frac{\delta\mathcal{F}}{\delta u} + \nu\partial_{xxt}u,\end{aligned} \tag{11}$$

where $\varepsilon = \partial\Phi/\partial\rho|_{\rho_M}$ is the control parameter and $\nu\partial_{xxt}u$ is a diffusion term. The variables scale as $u \sim \varepsilon^{1/2}$, $j \sim \varepsilon$, $\partial_x \sim \varepsilon^{1/2}$, $\partial_t \sim \varepsilon$ and $\nu \sim o(1)$. Note that, the convection term in the momentum flux ($\frac{\partial\Phi}{\partial j^2}j^2 \sim \varepsilon^2$) has been neglected, in comparison with the dominant part (order $\varepsilon^{3/2}$). The sign of $\partial\Phi/\partial\rho_{xx}|_{\rho_M}$ has been chosen to be negative, in order to saturate the linear instability and to impose the existence of a global minimum for the free energy

$$\mathcal{F} = \int dx \left\{\varepsilon\frac{u^2}{2} + \frac{u^4}{4} + \frac{(\partial_x u)^2}{2}\right\}. \tag{12}$$

Eq. (11), that describes the time evolution of the system close to the critical point, implies that the system evolves in a irreversible manner toward an stationary state characterized by the minimization of the $\mathcal{F}$. It can be directly checked form Eq. (11) that $(\mathcal{K}+\mathcal{F})$ decreases monotonically, where $\mathcal{K}=\int dx(\partial_t \Lambda)^2$ and Λ is the primitive of u. Then, the final state is stationary and with the minimum value of $\mathcal{F}$. Also, is a small noise were added to the equation (to describe fluctuations) it can be shown that the stationary probability distribution of u is of the form $P(u)\sim e^{-\mathcal{F}[u]/\eta}$, where η is the noise intensity [26–28]. These properties make appropriate to call $\mathcal{F}$ a *free energy* or a *Lyapunov functional*.

The study of instabilities in non-linear physics have shown that the existence of a non-equilibrium free energy, allows to use some concepts of equilibrium thermodynamics in non-equilibrium instabilities. In particular, Maxwell's construction can be used to determine the coexisting densities. Also, the structure of $\mathcal{F}$ indicates that large density gradients (thus interfaces) are energetically suppressed.

We emphasize that the Landau free energy $\mathcal{F}$ has the classical phase diagram, with coexistence and spinodal curves [29]; as those observed in binary fluids, binary alloys, and $^3He-^4He$ mixtures, to mention a few examples (see [5] and references cited therein).

For negative ε, the homogeneous solution ($u=0$) undergoes a spatial instability, characterized by the appearance of equally distributed bubbles. Later on, closest bubbles merge into a bigger one, as a consequence of a coalescence process. Subsequently, bubble dynamics is led by the interaction mediated by waves (see Figs. 4 and 5). The above dynamics is a consequence of the system tendency to minimize its free energy (see Ref. [30] for a complementary discussion). With periodic boundary conditions, the global minimum is a unique bubble, as the solution shown in Fig. 3. Further work in this coarsening process is in progress.

In the metastability region (see Fig. 6), i.e. the region bounded by the spinodal and coexistence curves, the homogeneous state is stable. Nevertheless, a finite fluctuation that overcomes the nucleation barrier gives rise to a bubble along with two *state-waves (densification waves)*, which propagate away from the bubble (see Fig. 3). These fronts are a result of mass conservation: when the bubble is created the excess mass must be ejected. Due to the periodic boundary conditions, later on, the waves collide with the bubble producing its oscillation. Afterward, due to viscosity, the oscillations are damped and the final state is a single bubble at rest.

It has been shown in a full linear stability analysis of the hydrodynamic equations that for aspect ratios $\lambda=L_x/L_y$ smaller than a critical value, the instability is suppressed [6, 16, 31]. The fact that the system becomes stable for small enough values of λ is also captured in the van der Waals equation. A linear stability analysis of Eq. 11 around the homogeneous state shows that the perturbations with wave-vectors larger than $k^c=\sqrt{-\varepsilon-3u_0^2}$ are stable, where u_0 is the reference scaled density. Then, if the horizontal system size is

smaller than $L_x^c = 2\pi/k^c$, the system is always stable. This is an effect of the surface energy already mentioned. We have used this result to compute the van der Waals loops in thin columns.

The numerical solutions of Eq. (11) (see Figs. 3 and 4) in the unstable and metastable regions show good qualitative agreement with the molecular dynamic simulations. That is, the model captures the main features of the system dynamics close to the instability (density waves, fronts, metastability, and instability).

The model (11) implies also that for global densities smaller than the Maxwell point density ($u < 0$), dense regions (instead of low density regions) can nucleate. This prediction is in agreement with the simulations presented in Fig. 5, where one or many dense regions are nucleated for $n_0 < 0.05$. The dynamics of $\rho(x,t)$ is, however, not completely well described by the model because these simulations are done with parameters not close to the critical point. The case of $n_0 = 0.03$ is special, because in this case a long wavelength density modulation is created before the droplet appears. This phenomenon is not captured by the model.

In experiments there is always a small amount of friction with the air or the walls. In this case momentum is not exactly conserved and the model must be modified. The momentum density satisfies the following equation

$$\partial_t j = -\partial_x \Phi - \mu j, \tag{13}$$

where μ is the friction coefficient. Inserting (13) into (9a) and doing the appropriate scalings we obtain the modified van der Waals equation

$$\partial_{tt} u + \mu \partial_t u = \partial_{xx} \left(\varepsilon u + u^3 - \partial_{xx} u + \nu \partial_t u \right). \tag{14}$$

If μ is large, the above equation reduces adiabatically to the usual Cahn-Hilliard equation [29] that differs from the van der Waals equation in that it does not present waves and the dynamics is much slower (see Appendix). Note that, usual spinodal decomposition in binary mixtures, for example, obeys the Cahn-Hilliard and not the van der Waals equation. Therefore, in experiments, the detection of density and shock waves will depend on the intensity of the friction. In Fig. 7 the time evolution of the spinodal decomposition process with and without friction is presented. In both cases noise is added (see Appendix) to trigger nucleation. In the case without friction waves are observed and the coarsening evolution is faster, while in the case with friction waves are almost suppressed. Also, the coarsening process is much slower in this case.

As a final test of the model, we have made MD simulations of the system in the elongated box setup (extended system). For two global densities ($n_0 = 0.08$ and $n_0 = 0.15$) and a number of different inelasticities, the systems were simulated until a final steady state is achieved with one or no bubble inside. When the final configuration contained one bubble (or droplet) the vertical-averaged density profile $\rho(x)$ was extracted. In the Ginzburg-Landau theory

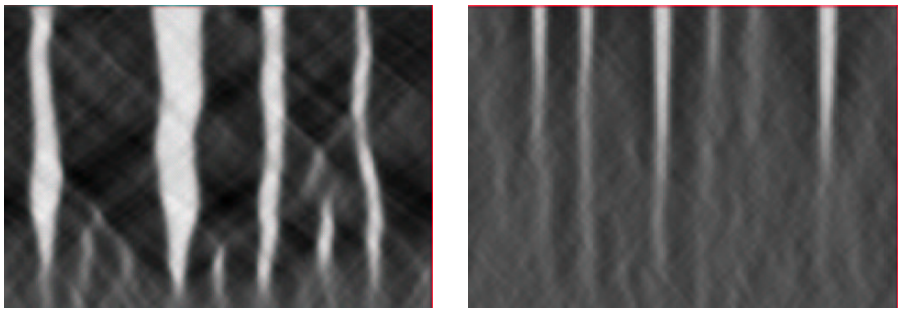

Fig. 7. Spatiotemporal evolution of the coarse grained density in the unstable region, modeled by Eq. (16). **Left**: $\varepsilon = -0.51$, $\nu = 0.5$, $\eta_0 = 0.5$, and $\mu = 0.0$. **Right**: the same parameters but with moderate friction connected, $\mu = 0.3$.

[32] it is shown that the density profile that minimizes the Landau free energy (12) is a single bubble were the kink profile is given a by an hyperbolic tangent. Then, we fit $\rho(x)$ to

$$\rho(x) = \rho_1 + \frac{\rho_2 - \rho_1}{2}\left[\tanh\left(\frac{x - x_A}{\Delta_x}\right) - \tanh\left(\frac{x - x_B}{\Delta_x}\right)\right] \tag{15}$$

where ρ_1 and ρ_2 are the homogeneous densities of the two phases, Δ_x is the interface width, and x_A and x_B are the position of the kinks (bubble borders).

In each case we computed also the vertical average of the horizontal component of the pressure tensor p_{xx}. Even in the presence of bubble, it is horizontally homogeneous, as the system is is mechanical equilibrium.

The homogeneous densities ρ_1 and ρ_2 should correspond to the coexistence densities of the van der Waals theory. In Fig. 8 we present these densities as a function of the homogeneous pressure p_{xx}. We note that the coexisting densities in both series of simulations (made with different global densities) coincide. Also the final pressure depends only on the inelasticity q, but not on the global density. These results confirm that the phenomenon is a van der Waals separation.

The coexisting densities are compared in Fig. 8 with the predictions obtained using Maxwell's construction in the simulation on tall columns. The comparison is fairly good indicating that the phenomenological Landau free energy (12), from where we made the Maxwell construction, is qualitatively correct even far from the critical point.

In summary, we have studied the phase separation in fluidized granular matter. Molecular dynamics simulations of a grain system, in two dimensions, with a vibrating wall and no gravity exhibit appearance, coagulation and disappearance of low density regions (bubbles). Rarefaction and densification density waves lead the bubble dynamics. The mechanism of phase separation is triggered by a negative compressibility which, in turns, is a result of the

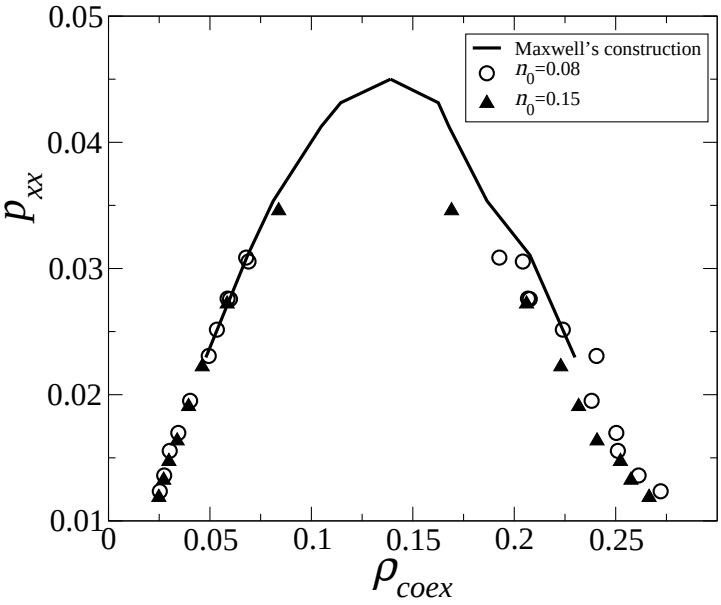

Fig. 8. Coexistence densities ρ_{coex} as a function of the $x - x$ component of the pressure tensor. Symbols are results obtained in MD simulations of extended systems for two global densities: $n_0 = 0.08$ and $n_0 = 0.15$. Different points correspond to different inelasticities. The continuous line is the prediction obtained from the Maxwell construction extracted from the simulations in tall columns.

fact that for granular media in closed geometries the granular temperature is a decreasing function of the density.

A simple hydrodynamic model is able to predict the existence of van der Waals loops in the effective pressure. The predicted critical point is in qualitative agreement with the results of molecular dynamic simulations.

Close to the transition, the system is described by the van der Waals normal form (11). This model describes quite well the molecular dynamics simulations. The phase separation is the analog to the spinodal decomposition of the gas-liquid transition of the van der Waals model, but the transient evolution of the system is led by state-waves.

The van der Waals instability should be observed independently of the peculiarities of the energy injection mechanism or of its stochastic modelization, as long as the particle collisions with the wall conserve horizontal momentum. It should also be observed in the presence of a small gravitational field either by inclining slightly the table or by placing the system vertically with characteristic injected energy much larger than the gravitational potential energy ($m(A\omega)^2 \gg mgL_y$). In both possible generalizations, the general theoretical framework continues to be valid, and preliminary numerical simulations confirm it (in preparation).

The authors would like to thank P. Cordero, D Risso, and E. Tirapegui for fruitful discussions. The simulation software developed at INLN, France, has been used for the simulations of model (11). M.G.C. and R.S. thank the support of *Programa de inserción de científicos chilenos* of Fundación Andes and the support of FONDAP grant 11980002. M.A. and R.S. greatly thank the support of the FONDECYT projects 30000017 and 1010416, respectively.

References

[1] P. B. Umbanhowar, F. Melo, and H. L. Swinney, Nature **382**, 793 (1996).
[2] R. Ramírez, D. Risso, and P. Cordero, Phys. Rev. Lett. **85**, 1230 (2000).
[3] Y. Forterre and O. Pouliquen, Phys. Rev. Lett. **86**, 5886 (2001).
[4] M-L. Tan and I. Goldhirsch, Phys. Rev. Lett. **81**, 3022 (1998); L. Kadanoff, Rev. Mod. Phys. **71**, 435 (1999). B.J. Glasser and I. Goldhirsch, Phys. Fluids **13**, 407 (2001).
[5] J. D. Gunton, M. San Miguel, and P. S. Sanhi, in *Phase Transitions and Critical Phenomena, volume 8*, edited by D. Domb and J. L. Lebowitz (Academic Press, London, 1983), pp. 267–466.
[6] E. Livne, B. Meerson, and P.V. Sasorov, Phys. Rev. E **65**, 021302 (2002).
[7] J. J. Brey, F. Moreno, and R. García-Rojo, M. J. Ruiz-Montero, Phys. Rev. E **65**, 061302 (2002).
[8] M. Argentina, M. Clerc, and R. Soto, Phys. Rev. Lett. **89**, 044301 (2002).
[9] S. Warr and J. M. Huntley, Phys. Rev. E **52**, 5596 (1995).
[10] I. Goldhirsch and G. Zanetti, Phys. Rev. Lett. **70**, 1619 (1993).
[11] P. Zamankhan, A. Mazouchi, and P. Sarkomaa, Appl. Phys. Lett. **71**, 3790 (1997).
[12] D. C. Rapaport, Physica A **249**, 232 (1998).
[13] E. L. Grossman, T. Zhou, and E. Ben-Naim, Phys. Rev. E **55**, 4200 (1997).
[14] L. D. Landau and E. M. Lifshitz, *Statistical Physics* (Pergamon Press, New York, 1969).
[15] This mechanism is similar to the one giving rise to the clustering phenomena [10]. Nevertheless, is this later case the granular temperature is not an slave variable.
[16] E. Khain and B. Meerson, Phys. Rev. E **66**, 021306 (2002).
[17] J. J. Brey, M. J. Ruiz-Montero, F. Moreno, and R. García-Rojo, Phys. Rev. E **65**, 011305 (2002).
[18] J. T. Jenkins and M. W. Richman, Arch. Rat. Mech. **87**, 355 (1985).
[19] J. J. Brey, F. Moreno, and J. W. Dufty, Phys. Rev. E **54**, 445 (1996).
[20] C. Bizon, M. D. Shattuck, J. B. Swift, and H. L. Swinney, Phys. Rev. E **60**, 4340 (1999).
[21] R. Soto, M. Mareschal, and D. Risso, Phys. Rev. Lett. **83**, 5003 (1999).
[22] D. Gass, J. Chem. Phys **54**, 1898 (1971).
[23] S. Chapman and T. G. Cowling, *The Mathematical Theory of Non-Uniform Gases*, 3rd ed. (Cambridge University Press, New York, 1970).
[24] N. V. Brilliantov and T. Pöschel, *Kinetic Theory of Granular Gases*, (Oxford University Press, 2004).
[25] C. Cercignani, *Theory and Application of the Boltzmann Equation* (Elsevier, Amsterdam, 1975).

[26] M. S. Green, J. Chem. Phys. **20**, 1281 (1952).
[27] H. Grabert, R. Graham, and M. S. Green, Phys. Rev. A **21**, 2136 (1980).
[28] M. C. Cross and P. C. Hohenberg, Rev. Mod. Phys. **65**, 851 (1993).
[29] J. W. Cahn and J. E. Hilliard, J. Chem. Phys. **28**, 258 (1958).
[30] E. Livne, B. Meerson, and P.V. Sasorov, Phys. Rev. E **66**, 050301(R) (2002).
[31] B. Meerson, T. Poöschel, P. V. Sasorov, and T. Schwager,`cond-mat/0208286`, (2002).
[32] K. Kawasaki , Prog. Theor. Phys. **79**, 161 (1984); Prog. Theor. Phys. **80**, 123 (1984).
[33] L. D. Landau and E. M. Lifshitz, *Fluid Mechanics*, Pergamon Press, Oxford (1984).

A Density fluctuations

Density fluctuations are a important aspect of the described phenomenon. They are responsible for the nucleation of bubbles in the metastable region. Also, in the homogeneous phases, they seem to propagate with well defined velocities (see Figs. 3-5). The dynamics of these fluctuations can be understood using the van der Waals model. A study of the system dynamics close to the instability threshold, where noise is amplified was done in Ref. [31].

In fact, density fluctuations are created by internal noise, and they obey the linearized van der Waals equation, with the addition of a noise term. In the spirit of Landau and Lifshitz's theory [33], the noise term must be added to the constitutive relation (10). If n_0 is the homogeneous density, the density fluctuations $n(x,t) = \rho(x,t) - n_0$ and the momentum density $j(x,t)$ are described by

$$\begin{aligned} \partial_t n &= -\partial_x j \\ \partial_t j &= -\partial_x \left(cn - \partial_{xx} n - \nu \partial_x j \right) - \mu j - \partial_x \eta \end{aligned} \tag{16}$$

where $\eta(x,t)$ is a noise term and $c = \varepsilon + 2n_0^2$.

The above equations can be solved in Fourier space $n(x,t) = n_k(t)e^{ikx}$, $j(x,t) = j_k(t)e^{ikx}$, in terms of the noise. The statistical properties of the noise are unknown, especially because the reference system is out of equilibrium and fluctuation-disipation theorems cannot be applied. However, close to the critical point the only slow variables are the order parameters, all the others having fast dynamics and short correlation times. Then, close to the critical point, it can be safely assumed that the noise is white and delta correlated in space. That is, we assume that $\langle \eta_k(t)\eta_{k'}(t')\rangle = \eta_0 \delta(t-t')\delta(k+k')$.

The statistical properties of the density fluctuations are obtained computing the intermediate scattering function

$$F(k,t) = \lim_{t' \to \infty} \langle n_k(t+t') n_{-k}(t') \rangle \tag{17}$$

where the average is over realizations. With the assumption of white noise it reduces to

$$F(k,t) = \eta_0 k^2 \int_0^\infty ds \left[e^{A_k(t+s)}\right]_{12} \left[e^{A_{-k}s}\right]_{12} \tag{18}$$

where the matrix A_k is

$$A_k = \begin{pmatrix} 0 & -ik \\ -ikc - ik^3 & -\mu - \nu k^2 \end{pmatrix} \tag{19}$$

and the subscript 12 means that this component of the matrix must be taken.

The instantaneous density fluctuations are described by

$$F(k) = F(k,0) = \frac{\eta_0 k^2}{2(c+k^2)(\mu+\nu k^2)} \tag{20}$$

that has a maximum at $k^* = (c\mu/\nu)^{1/4}$. Note that if there is no friction ($\mu = 0$) long wavelength fluctuations are the predominant ones.

The time evolution of the density fluctuations are given by the eigenvalues of A_k, that can be real or complex conjugate. In the real case, the evolution is purely diffusive, while in the complex case waves propagate. For a given wave-vector k, waves propagate if

$$4(ck^2 + k^4) - (\mu + k^2\nu)^2 > 0, \tag{21}$$

condition that is fulfilled in general when the dissipation mechanisms (μ and ν) are small. The critical condition for the suppression of all waves is that

$$\nu = \frac{c^2 + \mu^2}{c\mu} \tag{22}$$

when all fluctuations diffuse. Note that in the Cahn-Hilliard limit ($\mu \to \infty$) the evolution, then, is simply diffusive. In Fig. 9 numerical solutions of the Eq. (16) are presented. It is seen that when friction is connected ($\mu \neq 0$), waves are suppressed and the evolution is diffusive.

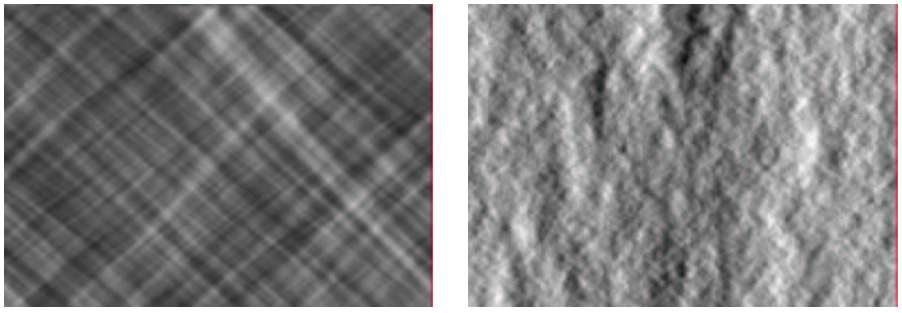

Fig. 9. Spatiotemporal evolution of the density fluctuations in the stable region, modeled by Eq. (16). **Left**: $\varepsilon = 0.47$, $\nu = 0.1$, $\eta_0 = 0.5$, and $\mu = 0.0$. **Right**: the same parameters but with friction connected, $\mu = 0.52$.